

The Stable Explicit Time Stepping Analysis with a New Enrichment Scheme by XFEM

Xue-cong Liu¹, Qing Zhang^{1,2} and Xiao-zhou Xia¹

Abstract: This paper focuses on the study of the stability of explicit time integration algorithm for dynamic problem by the Extended Finite Element Method (XFEM). A new enrichment scheme of crack tip is proposed within the framework of XFEM. Then the governing equations are derived and evolved into the discretized form. For dynamic problem, the lumped mass and the explicit time algorithm are applied. With different grid densities and different forms of Newmark scheme, the Dynamic Stress Intensity Factor (DSIF) is computed by using interaction integral approach to reflect the dynamic response. The effectiveness of the proposed scheme is demonstrated through the numerical examples, and the critical time stepping in different situations are listed and analyzed to illustrate the factors that affect stability.

Keywords: XFEM, DSIF, newmark scheme, time stepping, stability.

1 Introduction

The fracture analysis of structures and components has been widely applied and highly valued in recent years, and modeling discontinuities like crack is one of the important parts in the simulation of failure. In order to model the crack and crack growth behavior, the way of remeshing is used by classic finite element method (FEM) in order to align the mesh with discontinuities. In addition, other solutions such as meshfree method, boundary element method and extended finite element method (XFEM) are available.

As proposed by Belytschko and Black (1999); Noes, Dolbow and Belytschko (1999); Belytschko and Noes (2001), XFEM based on the concept of partition unity becomes a dominant numerical scheme. The crack can be modeled independent of finite element mesh. All the elements are divided into the normal parts and the enriched parts. Since the elements can be influenced directly by crack, the enrich functions are introduced. Heaviside function and the Westergaard stress function are used frequently for the discontinuities and the tip's stress singularity, respectively. XFEM is used to simplify the discontinuous problems and perform well in stress analysis concerned with fracture mechanics.

Dealing with the dynamic fracture, Belytschko, Chen, Xu et al. (2003) proposed a tip element in which the crack opens linearly and developed a propagation criterion with loss of hyperbolic. Later on, a singular tip enrichment function is proposed for the elastodynamic

¹ Department of Engineering Mechanics, Hohai University, No. 8 Focheng West Road, Nanjing 210098, China.

² E-mail: lxzhangqing@hhu.edu.cn.

cracks with explicit time integration scheme [Belytschko and Chen (2004)]. In order to deeply study the stability and energy conservation to get a more accurate result, Réthoré, Gravouil and Combescure (2005a, 2005b) combined Space and Time XFEM (STX-FEM) to obtain a unified space-time discretization, and concluded that the STX-FEM is a suitable technique for dynamic fracture problems. On the other hand, a new lumping technique for mass matrix was proposed in order to be more suitable for dynamic problems by Menouillard, Réthoré, Combescure et al. (2006); Menouillard, Réthoré, Noes et al. (2008) and the robustness and stability of the approach has been proved.

As we noticed, the previous study is all based on the classical enrichment scheme, and a large number of additional degrees of freedom (DOFs) are required. In the meantime, various improved enrichment methods have been studied. Song, Areias and Belytschko (2006) has reinterpreted the conventional displacement field, described discontinuities by using phantom nodes and superimposed extra elements onto the intrinsic grid for dynamic fracture problems. The method doesn't require subdomain integration for the discontinuous integrand and has a highly efficient but nevertheless quite accurate formulation. Further, Duan, Song, Menouillard et al. (2009) has shown its practicability on the shell problem as well as three-dimension problem [Song and Belytschko (2009)]. Besides, changing the basic enrichment function is another solution. Menouillard, Song, Duan et al. (2010) proposed a new enrichment method with only a singular enrichment, which shows great accuracy for stationary cracks. The similar research has been done by Rabczuk, Zi and Geretenberger et al. (2008). Without crack tip enrichment, the Heaviside function has also been improved. Nistor, Pantale and Capone (2008) used only Heaviside function to model the dynamic crack growth. Kumar, Singh, Mishra et al. (2015) presented a new approach based Heaviside function along with a ramp function which contains information like crack length and angle. A similar method was proposed by Wen and Tian (2016); Tian and Wen (2016), which is based on an extended free partition of unity enrichment technique, and no more extra DOFs are added in the dynamic crack growth simulation.

For all the study discussed above, the stability of the method is always concerned. Generally, using explicit scheme for dynamic problem, one goes through a very small time stepping that leads to high computation cost, while with a larger one the numerical result may be divergent. In the present paper, we will focus on the stability of the numerical scheme. A new enrichment scheme is used for the elements influenced by crack tip based on the analytical solution of the displacement fields near crack tip. The Newmark scheme is adopted for time integration, and different parameters are tested to investigate their influence on the stability. In addition, DSIF is calculated as an important parameter which represents the variation of the stress field around the crack tip, and also can determine the stability of the simulation.

This paper is organized as following: Section 2 illustrates the governing equations and the XFEM; The explicit time algorithm and the lumping technique are introduced in Section 3; The DSIF is shown in Section 4; In Section 5, in order to verify the feasibility and accuracy of the simulation, several numerical examples are provided.

2 Governing equations and XFEM formulation

2.1 Governing equations

In order to develop the equations governing the problem, a homogeneous two-dimensional domain Ω with cracks is considered. As described in Figure 1, the domain Ω is bounded by Γ which is composed of Γ_u , Γ_t and Γ_c . Throughout this paper, prescribed displacements are imposed on Γ_u , while traction is imposed on Γ_t . Γ_c is referred to as the crack surface and assumed to be traction-free. The strong form of the linear momentum equation and the boundary conditions are

$$\nabla \cdot \boldsymbol{\sigma} + \mathbf{b} = \rho \ddot{\mathbf{u}} \quad \text{in } \Omega \quad (1a)$$

$$\mathbf{u} = \bar{\mathbf{u}} \quad \text{on } \Gamma_u \quad (1b)$$

$$\boldsymbol{\sigma} \cdot \mathbf{n} = \bar{\mathbf{t}} \quad \text{on } \Gamma_t \quad (1c)$$

$$\boldsymbol{\sigma} \cdot \mathbf{n} = 0 \quad \text{on } \Gamma_c \quad (1d)$$

$$\boldsymbol{\varepsilon} = \nabla_s \mathbf{u} \quad (1e)$$

$$\boldsymbol{\sigma} = \mathbf{C} : \boldsymbol{\varepsilon} \quad (1f)$$

where $\boldsymbol{\sigma}$ is prescribed the Cauchy stress tensor, \mathbf{u} and $\ddot{\mathbf{u}}$ are the displacement field vector and the vector of acceleration, respectively. \mathbf{b} is the body force vector, ρ is the mass density, $\bar{\mathbf{u}}$ is the prescribed displacement, \mathbf{n} is the unit outward normal, ∇_s is the symmetric operator, \mathbf{C} is the elastic module tensor and $\boldsymbol{\varepsilon}$ is the strain tensor. In the present investigation, we consider the small strains and displacements as shown in Eq.(1e). Using the equilibrium momentum equation and the constitutive relation in the weak form, we have

$$\int_{\Omega} \delta \nabla_s \mathbf{u}^T : \mathbf{C} : \nabla_s \mathbf{u} d\Omega + \int_{\Omega} \rho \ddot{\mathbf{u}} \delta \mathbf{u} d\Omega = \int_{\Omega} \delta \mathbf{u} \cdot \mathbf{b} d\Omega + \int_{\Gamma_t} \delta \mathbf{u} \cdot \bar{\mathbf{t}} d\Gamma \quad (2)$$

2.2 The XFEM formulation

Consider a typical finite element mesh with four-node elements as shown in Fig.2, in which the geometry of crack is independent of the mesh. As in the classical XFEM, the nodes by Heaviside enrichment are enriched with two addition DOFs, and the shape functions are constructed from the Heaviside function $H(x)$. $H(x)$ is defined as a unit magnitude for the elements cut completely by crack, and takes ± 1 on the two sides of the crack. For the nodes with crack tip enrichment, they are enriched frequently by eight addition DOFs. The basic enrichment functions are inspired from the near tip displacement fields of mode I and mode II cracks in FEM, and can be written as the functions $\boldsymbol{\psi}_k(r, \theta)$ [Belytschko and Black (1999)].

$$\psi_k(r, \theta) = \sqrt{r} \left\{ \cos\left(\frac{\theta}{2}\right), \sin\left(\frac{\theta}{2}\right), \sin\left(\frac{\theta}{2}\right)\cos(\theta), \cos\left(\frac{\theta}{2}\right)\sin(\theta) \right\} \quad k=1,2,3,4 \quad (3)$$

where (r, θ) are the local polar coordinates at the crack tip. We note that the second function in Eq. (3) is commonly referred to branch function, while the others are continuous and added to improve the accuracy. Besides, $\psi_k(r, \theta)$ can be presented with other function set or just with the branch function, and it is well-documented and verified by Dolbow, Noes and Belytschko (2000).

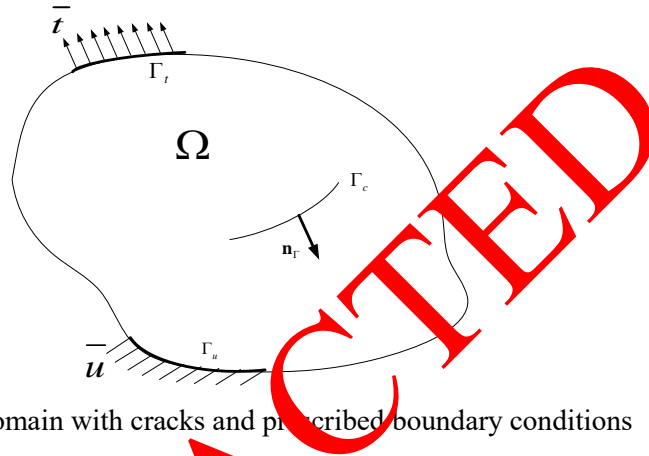


Figure 1: Domain with cracks and prescribed boundary conditions

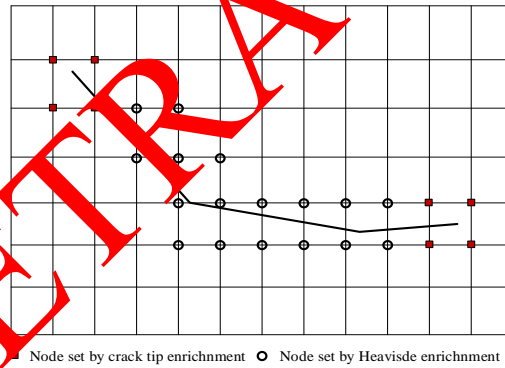


Figure 2: Typical discretization of a domain with crack and enriched nodes by XFEM

As mentioned above, the enrichment functions are developed based the asymptotic displacement fields of the crack tip, and can take different forms. In the present paper, a new form of enrichment functions is used, which derives from the asymptotic displacement fields directly. By shifting the enrichment functions, we are able to correspond the enriched nodes' displacement to the true displacement with XFEM. The displacement can be written approximately as

$$\mathbf{u}(x) = \sum_{i \in I} N_i(x) \mathbf{u}_i + \sum_{j \in J} N_j(x) [H(x) - H(x_j)] \mathbf{a}_j + \sum_{k \in K} N_k(x) \mathbf{B}_T [\mathbf{F}(x) - \mathbf{F}(x_k)] \mathbf{b}_k \quad (4)$$

where I is the set of all nodes in the mesh, J is the set of nodes enriched by Heaviside

function and K is enriched by $\mathbf{F}(x)$. $N_i(x)$ is shape functions of finite element. \mathbf{a}_j and \mathbf{b}_k are the addition DOFs associated with $H(x)$ and $\mathbf{F}(x)$, respectively. β_T is the transformation matrix between the local coordinate and global coordinate. $\mathbf{F}(x)$ is the crack tip function in matrix form

$$\mathbf{F}(x) = \frac{1}{2G} \sqrt{\frac{r}{2\pi}} \begin{bmatrix} \cos\frac{\theta}{2}(\kappa - \cos\theta) & \sin\frac{\theta}{2}(\kappa - 2 + \cos\theta) \\ \sin\frac{\theta}{2}(\kappa - \cos\theta) & \cos\frac{\theta}{2}(\kappa - 2 + \cos\theta) \end{bmatrix} \quad (5)$$

where G is the shear modulus of material, $G = \frac{E}{2(1+\nu)}$. E is the modulus of

elasticity, ν is the Poisson's ratio. κ is the Kolosov constant $\kappa = \begin{cases} 3-4\nu, & \text{plane strain} \\ \frac{3-\nu}{1+\nu}, & \text{plane stress} \end{cases}$.

It is important to point out that although $\mathbf{F}(x)$ still has 4 base functions, the number of additional DOFs is reduced from 8 to 2 for the nodes enriched by crack tip. The two base functions in first row of matrix $\mathbf{F}(x)$ are associated with the horizontal axis in the local coordinate at crack tip, and the second row corresponds to the vertical axis.

Without concerning the damping effect, we substitute the displacement field Eq. (4) into the weak form Eq. (2). It then yields a system of linear algebraic matrix equations, which can be expressed as

$$\mathbf{M}\ddot{\mathbf{U}} + \mathbf{K}\mathbf{U} = \mathbf{f} \quad (6)$$

where \mathbf{M} is the mass matrix, \mathbf{K} is the stiffness matrix and \mathbf{f} is the force matrix:

$$\mathbf{M} = \begin{bmatrix} \mathbf{M}^{uu} & \mathbf{M}^{ua} & \mathbf{M}^{ut} \\ \mathbf{M}^{au} & \mathbf{M}^{aa} & \mathbf{M}^{at} \\ \mathbf{M}^{tu} & \mathbf{M}^{ta} & \mathbf{M}^{tt} \end{bmatrix} \quad (7.a)$$

$$\mathbf{K} = \begin{bmatrix} \mathbf{K}^{uu} & \mathbf{K}^{ua} & \mathbf{K}^{ut} \\ \mathbf{K}^{au} & \mathbf{K}^{aa} & \mathbf{K}^{at} \\ \mathbf{K}^{tu} & \mathbf{K}^{ta} & \mathbf{K}^{tt} \end{bmatrix} \quad (7.b)$$

$$\ddot{\mathbf{U}} = [\ddot{\mathbf{u}} \quad \ddot{\mathbf{a}} \quad \ddot{\mathbf{t}}]^T, \quad \mathbf{U} = [\mathbf{u} \quad \mathbf{a} \quad \mathbf{t}]^T, \quad \mathbf{f} = [\mathbf{f}^u \quad \mathbf{f}^a \quad \mathbf{f}^t]^T \quad (7.c)$$

The sub-matrices and vectors that come in the foregoing equations are defined as below for four-node element ($i, j = 1, 2, 3, 4$):

$$\mathbf{M}_{ij}^{rs} = \int_{\Omega^e} \rho (\mathbf{N}_i^r)^T \mathbf{N}_j^s d\Omega, \quad r, s = u, a, t \quad (8)$$

$$\mathbf{K}_{ij}^{rs} = \int_{\Omega^e} (\mathbf{B}_i^r)^T \mathbf{B}_j^s d\Omega, \quad r, s = u, a, t \quad (9)$$

$$\mathbf{f}_i^u = \int_{\Omega} N_i \mathbf{b} d\Omega + \int_{\Gamma_i} N_i \bar{\mathbf{t}} d\Gamma \quad (10.a)$$

$$\mathbf{f}_i^a = \int_{\Omega} N_i [H(x) - H(x_i)] \mathbf{b} d\Omega + \int_{\Gamma_i} N_i [H(x) - H(x_i)] \bar{\mathbf{t}} d\Gamma \quad (10.b)$$

$$\mathbf{f}_i^t = \int_{\Omega} N_i \boldsymbol{\beta}_T [\mathbf{F}(x) - \mathbf{F}(x_i)] \mathbf{b} d\Omega + \int_{\Gamma_i} N_i \boldsymbol{\beta}_T [\mathbf{F}(x) - \mathbf{F}(x_i)] \bar{\mathbf{t}} d\Gamma \quad (10.c)$$

where \mathbf{N}_i^a and \mathbf{N}_i^t are the matrices of additional shape functions in XFEM, \mathbf{B}_i^a and \mathbf{B}_i^t are the matrices of shape function derivatives and can be expressed as:

$$\mathbf{N}_i^a = N_i \begin{bmatrix} H(x) - H(x_i) & 0 \\ 0 & H(x) - H(x_i) \end{bmatrix} \quad (11.a)$$

$$\mathbf{N}_i^t = N_i \boldsymbol{\beta}_T [\mathbf{F}(x) - \mathbf{F}(x_i)] \quad (11.b)$$

$$\mathbf{B}_i^a = \begin{bmatrix} (N_i (H(x) - H(x_i)))_{,x} & 0 \\ 0 & (N_i (H(x) - H(x_i)))_{,y} \\ (N_i (H(x) - H(x_i)))_{,y} & (N_i (H(x) - H(x_i)))_{,x} \end{bmatrix} \quad (12.a)$$

$$\mathbf{B}_i^t = \begin{bmatrix} \frac{\partial}{\partial x} & 0 \\ 0 & \frac{\partial}{\partial y} (N_i \boldsymbol{\beta}_T [\mathbf{F}(x) - \mathbf{F}(x_i)]) \\ \frac{\partial}{\partial y} & \frac{\partial}{\partial x} \end{bmatrix} \quad (12.b)$$

3 The explicit time integration

3.1 Time integration

As the most commonly used for dynamic problems, the Newmark scheme is chosen as the time integration algorithm. As we know, the time integration algorithm can be divided into two types: the explicit and the implicit. With the implicit method, there is no intrinsic limit to the time step. But we need to solve the global equations by iterating in each step. For dynamic problems, lots of iterations are needed, which has many disadvantages such as vast computation and low efficiency by implicit scheme. Compared with the implicit scheme, the explicit scheme solves the equations independently with no iterative, which is chosen in this paper.

Two parameters β and γ are considered in the Newmark scheme and combined in Eq. (6).

The derived equation is given as

$$\mathbf{U}_{t+\Delta t} = \mathbf{U}_t + \Delta t \dot{\mathbf{U}}_t + \Delta t^2 \left(\frac{1}{2} - \beta \right) \ddot{\mathbf{U}}_t + \Delta t^2 \beta \ddot{\mathbf{U}}_{t+\Delta t} \quad (13.a)$$

$$\mathbf{M} \ddot{\mathbf{U}}_{t+\Delta t} = \mathbf{F}_{t+\Delta t} - \mathbf{K} \mathbf{U}_{t+\Delta t} \quad (13.b)$$

$$\dot{\mathbf{U}}_{t+\Delta t} = \dot{\mathbf{U}}_t + \Delta t (1 - \gamma) \ddot{\mathbf{U}}_t + \Delta t \gamma \ddot{\mathbf{U}}_{t+\Delta t} \quad (13.c)$$

where Δt is the time step, \mathbf{U}_t is the vector of displacement, $\dot{\mathbf{U}}_t$ and $\ddot{\mathbf{U}}_t$ are the vector of velocity and acceleration at time t , respectively.

For a numeric scheme, the stability, consistency and convergence are the main reference standard. As instability is a sufficient condition for non-convergence, the Newmark scheme and their stability are discussed in this paper. The stability conditions of Newmark scheme are deduced in detail by Réthoré, Gravouil and Combescure (2004) with their custom notations. They can concluded as

1. if $\frac{1}{2} \leq \gamma \leq 2\beta$, it is an unconditionally stable scheme.
2. If $\frac{1}{2} \leq \gamma$ and $2\beta \leq \gamma$, the stable condition is $\Delta t \leq \frac{1}{\omega_{\max} \sqrt{\frac{\gamma}{2} - \beta}}$.

where ω_{\max} is the maximum frequency of the structure.

As mentioned by Réthoré, Gravouil and Combescure (2004), if the parameters are chosen to be $\beta = \frac{1}{4}$ and $\gamma = \frac{1}{2}$, the updating equations are unconditionally stable. However, according to Eq. (13), if the acceleration item $\ddot{\mathbf{U}}_{t+\Delta t}$ exists in Eq. (13. a), the equations still need to be solved iteratively. Thus, for an explicit time integrator, $\beta = 0$ is used in the present paper. We noticed that if $\beta = 0$ and $\gamma = \frac{1}{2}$, the Newmark scheme evolves into the central difference method.

Furthermore, due to such a restriction of stability condition, there must be a critical time step Δt_c . With the time step Δt beyond the critical value, the numerical instability and convergence problem will happen at some point. In contrast, the numerical results are very stable within the critical time.

In this paper, we will focus on figuring out the critical time step, and finding out the factors that can affect it. Thus, tests with different grid densities and different parameters in the Newmark scheme will be conducted.

3.2 The lumped mass

The matrix above in Eq. (8) known as the consistent mass matrix, includes standard terms, block-diagonal enriched terms, and coupling terms [Menouillard, Réthoré, Combescure et al. (2006)]. However, for the problem of dynamic, the mass matrix lumped is used more

frequently in order to simplify the numerical calculations. Due to the existence of additional DOFs which have no clear physical significance, the distribution of mass is not just as a simple average as in traditional FEM. Menouillard, Réthoré, Noes et al. (2008) had in-depth study of the lumping technique for the mass matrix based on the conservation of mass and momentum, and proved its effectiveness with explicit scheme for dynamics by XFEM. Besides, the lumping technique was also researched by Zi, Chen, Xu et al. (2005); Elguedj, Gravouil and Maigre (2009); Song and Belytschko (2009); Jim, Zhang, Fang et al. (2016). In this paper, the lumped mass proposed by Menouillard, Réthoré, Combesure et al. (2006) is used

$$m_{\text{diag}} = \frac{m}{n_{\text{node}}} \frac{1}{\text{mes}(\Omega_e)} \int_{\Omega_e} H^2 d\Omega \quad (14)$$

where Ω_e is the element being considered, m is the element's mass, $\text{mes}(\Omega_e)$ is the area of element in 2D, n_{node} is the number of nodes in element, and H is the Heaviside function.

4 DSIF

As the relevant quantities of crack tip may be questionable on accuracy such as stress fields, the SIF based on energetic consideration is used as a parameter of the strength of singularity. There are a few schemes to calculate the SIF, such as the displacement extrapolation method, the virtual crack extension method, the virtual crack closure method and the interaction integral method. The interaction integral method is used here which has the highest accuracy according to the research of Nagashima, Omoto and Tani (2003). In the interaction integral method, the auxiliary fields are introduced and superimposed onto the actual fields.

For dynamic loading case, an item related to inertia is added, and the interaction integral with force-free on crack surface can be given as

$$I = \int_A (\sigma_{ij}^{\text{aux}} \varepsilon_{ij}^{\text{aux}} - \sigma_{ik}^{\text{aux}} \varepsilon_{ik} \delta_{lj}) q_{,j} dA + \int_A \rho \ddot{u}_i u_{i,l}^{\text{aux}} q dA \quad (15)$$

where $(\sigma_{ij}^{\text{aux}}, \varepsilon_{ij}^{\text{aux}}, u_i^{\text{aux}})$ and $(\sigma_{ij}^{\text{aux}}, \varepsilon_{ij}^{\text{aux}}, u_i^{\text{aux}})$ are the actual state and the auxiliary state, respectively. I is the interaction integral between the actual state and the auxiliary state, A is the integral domain. q is the weight function which is going to be 0 outside the contour boundary and is one inside in the present paper. The DSIF can be written as

$$\begin{cases} K_I = I^{\text{mode I}} \cdot E^*/2 \\ K_{II} = I^{\text{mode II}} \cdot E^*/2 \end{cases} \quad (16)$$

where E^* is equal to E for the plane stress and for the plane strain $E^* = E/(1-\nu^2)$.

The basic algorithm used here for the DSIF is concluded as following:

- (1) Give an integral rang R , then search for all the integral elements;
- (2) Loop through all the integral elements;

- (3) Loop through all the Gauss points in each integral element;
- (4) Calculate the actual state and the auxiliary state of each Gauss point;
- (5) Get the value of DSIF through Eq. (15) and Eq. (16).

where R is the ratio between the actual integral radius r and the minimum size L_{\min} of all elements as shown in Figure 3.

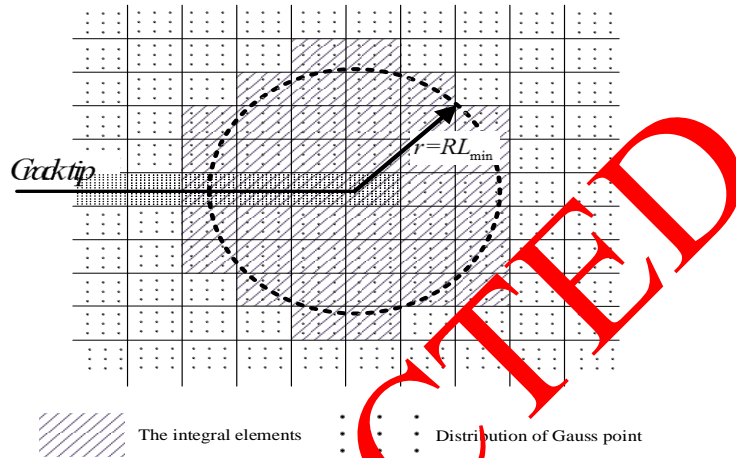


Figure 3: The integral elements for DSIF

5 Numerical examples

5.1 Stationary mode I crack

First, let us consider the problem of an infinite plate contains a semi-infinite crack whose geometry is shown in Figure 4. A theoretical solution of the problem was obtained by Freund (1990). To model this configuration, a rectangular plate of size $L \times 2H = 10 \times 4$ m with an initial edge crack of length $a = 5$ m under uniaxial tensile stress was used. The tensile stress was a type of Heaviside step loading, and $\sigma_0 = 500$ MPa. The material properties Young's modulus $E = 210$ Gpa, Poisson's ratio $\nu = 0.3$ and the density $\rho = 8000$ kg/m³. A mesh of 39×99 uniform square was used for tests. The theoretical DSIF of the problem with a stationary crack was given by Freund (1990):

$$K_I(t) = 2\sigma_0 \frac{\sqrt{c_d t(1-2\nu)/\pi}}{1-\nu} \quad (17)$$

where c_d is the dilatational wave speed, $t=0$ is the time stress wave reach the crack tip from the edge. The theoretical solution is used to compare our present results. Certainly, the theoretical solution has some limitation, and it is valid only at $t < 3t_c$ when the reflected stress wave reaches the crack tip. $t_c = H/c_d$ is the time that stress wave reaches the crack tip from the edge.

As time step is chosen as $\Delta t = 0.1 \mu s$, the values of DSIF with different integral path are presented in Figure 5. The DSIF was normalized by $K_0 = \sigma\sqrt{a}$ and compared with the theoretical solution. As shown in Figure 5, the results with different integral domains are in good agreement with each other. At $t < t_c$, the value of DSIF is 0 due to the stress wave has not reach the integral domain. The numerical solution is consistent with the theoretical solution after stress wave reaches the crack tip.

Figure 6 presents the results of DSIF with different time stepping Δt while $R=5$. It shows good consistency and the results are not sensitive to the time step. So, this inspires us to improve the computational efficient with a larger step time which is less than the critical time. With a much larger time stepping, $\Delta t = 20 \mu s$, the numerical result is rapidly divergent. As a consequence, there is a critical time stepping, which we will discuss it shortly.

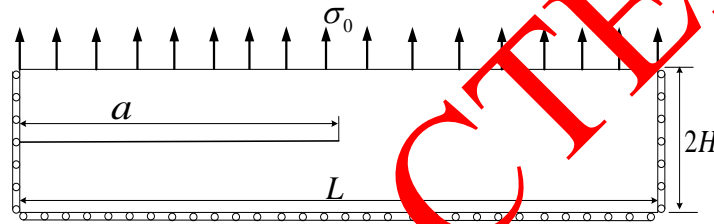


Figure 4: The geometry and loading of a homogeneous material plate with crack

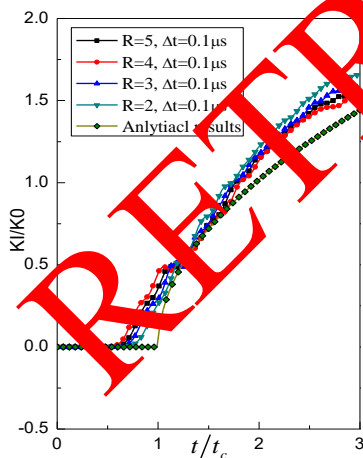


Figure 5: The DSIF with different integral path

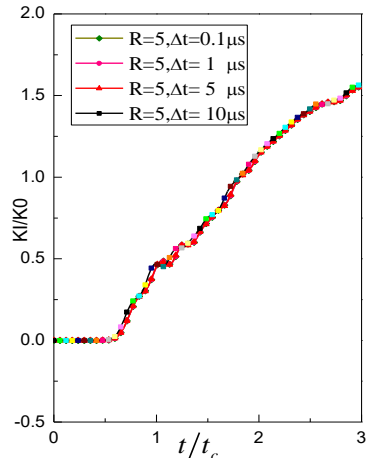


Figure 6: The DSIF with different time step

5.2 Finite size edge plate with an arbitrarily oriented central crack

A schema of the problem is shown in Figure 7. A plate with a central crack under uniaxial tensions $\sigma_0=100\text{MPa}$. The dimensions of the plate are $2h=0.04\text{ m}$ and $2b=0.02\text{ m}$, and the length of the central crack is $2a=0.0048\text{ m}$. The material's properties are: $E=199.99\text{Gpa}$, $\nu=0.3$, $\rho=5000\text{ kg/m}^3$. A mesh of 49×99 uniform elements is used.

First of all, $\theta=0^\circ$, a horizon central crack is considered. For the cases of different integral domains that affect the left crack tip, Figure 8 shows that the range R has little effect on the crack tip's DSIF. The results agree very well with the conclusion that the stress intensity factor under different integral path are the same. The numerical results with different time step are given in Figure 9, and the same conclusion can be drawn as shown in Figure 6.

Secondly, the central cracks of different inclined angle are considered. The length of crack is the same, and the angles, $\theta=15^\circ, 30^\circ, 45^\circ, 60^\circ, 75^\circ$ are examined. The problem has been discussed by Phan, Gray and Salvadori (2010) with Symmetric-Galerkin Boundary Element Method and by Liu, Bui, Zhang et al. (2012) with Smoothed Finite Element Method. The results are shown and compared with Phan, Gray and Salvadori (2010) in Figure 10. As depicted in Figure 10a, for the case of mode I, the values in the peak of DSIF curves decrease by the increase of θ for a small period of time after the stress wave arrive in the tip. Fig.10b reveals that DSIF in mode II are practically the same for the pair of $\theta=15^\circ$ and $\theta=75^\circ$, and the pair of $\theta=30^\circ$ and $\theta=60^\circ$. At the meanwhile, the curve of $\theta=45^\circ$ has the highest peak value.

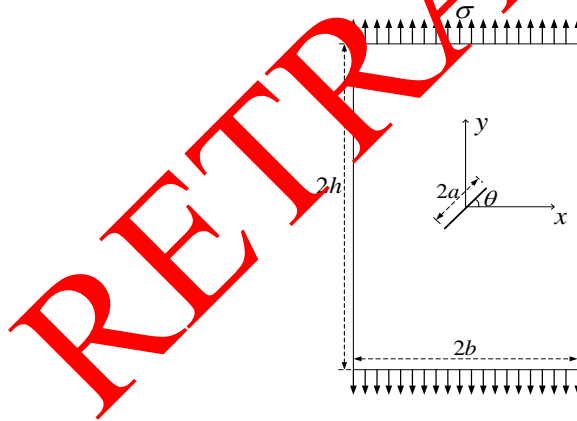


Figure 7: The rectangular plate with crack of different angle

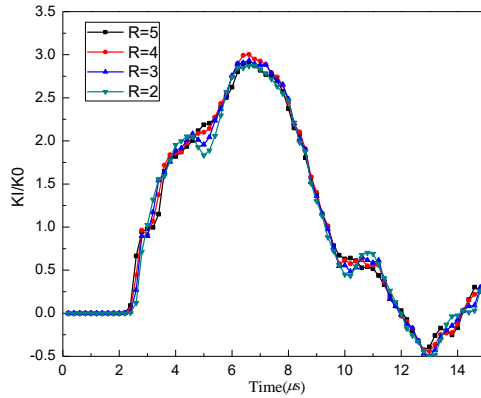


Figure 8: The DSIF with different integral path of the left crack tip

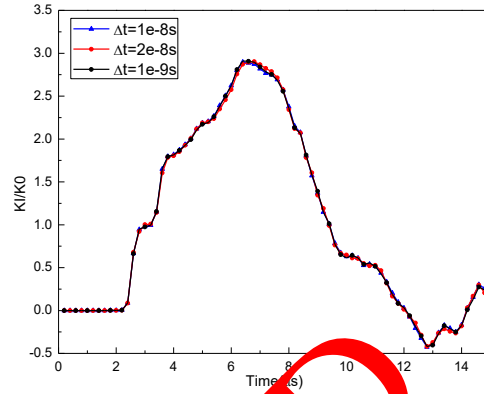


Figure 9: The DSIF of the left crack tip with different time increments

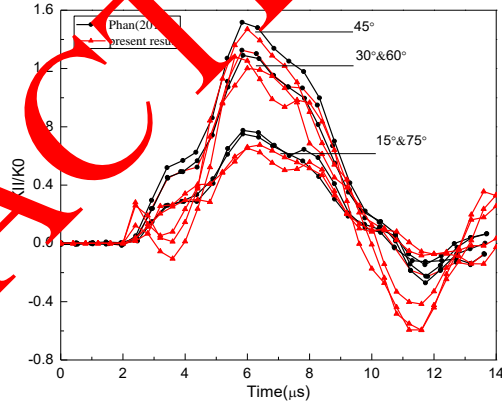
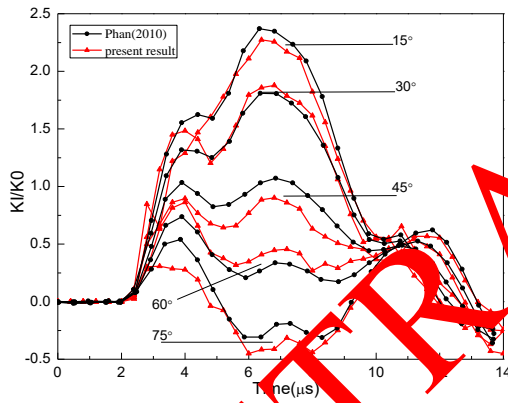


Figure 10: The DSIF of crack tip with different rotation angle: (a) Mode I; (b) Mode II

5.3 The stable explicit time stepping analysis

This part focuses on the main factors that influence the critical time step. The grid density and iteration form are the two main subjects. The experiment configuration model is presented in Figure 7 with $\theta=0^\circ$. The material properties and the other parameters are the same as that used in last example. In order to get the critical time Δt_c , the method of numerical approximation is used.

Firstly, the results were obtained with different grid densities. Three uniform meshes are considered, which are of CCT: 49×99 , CCT1: 24×49 , CCT2: 13×24 elements. With parameters $\beta=0$, $\gamma=1/2$ of Newmark scheme, the critical time step of different meshes can be turned out. As shown in Fig.11(a), the critical time we got is about $\Delta t_c = 4.825 \times 10^{-8}$ s with 49×99 elements. When the time step Δt is less than Δt_c , the numerical calculation results are completely consistent and do not produce divergence. Conversely,

divergence is presented in the calculation when $\Delta t > \Delta t_c$. The divergence occur at about $4.750 \mu\text{s}$, $7.154 \mu\text{s}$, $11.495 \mu\text{s}$, $15.141 \mu\text{s}$ when Δt is $5.000 \times 10^{-8} \text{s}$, $4.900 \times 10^{-8} \text{s}$, $4.850 \times 10^{-8} \text{s}$, $4.838 \times 10^{-8} \text{s}$, respectively. As a comparison, Figure 11(b) is presented with the mesh of 24×49 . It is seen that the critical time is $10.025 \times 10^{-8} \text{s}$ which is improved than the one in Figure 11(a). The divergence occurs at about $4.095 \mu\text{s}$, $9.494 \mu\text{s}$, $12.090 \mu\text{s}$, $17.085 \mu\text{s}$ when Δt is $10.500 \times 10^{-8} \text{s}$, $10.100 \times 10^{-8} \text{s}$, $10.075 \times 10^{-8} \text{s}$, $10.050 \times 10^{-8} \text{s}$, respectively.

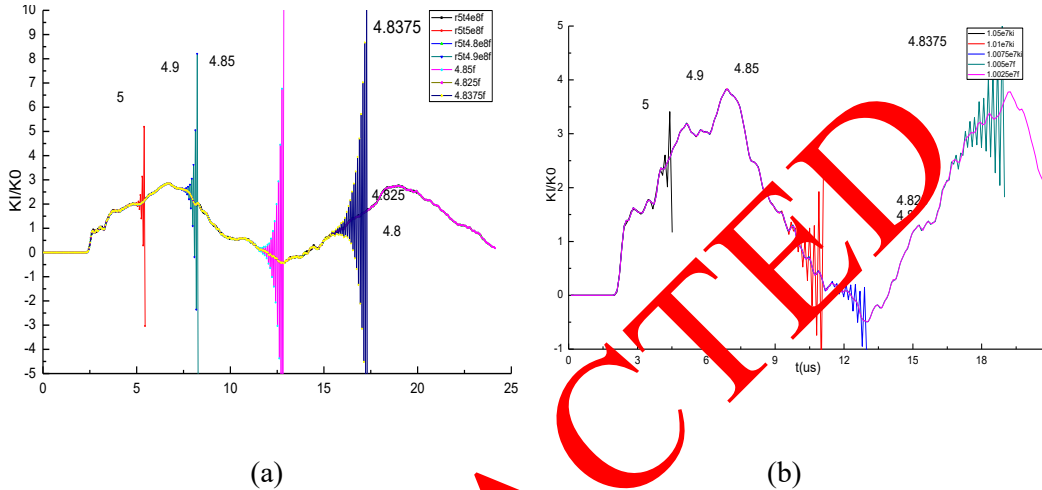


Figure 11: Numerical stability with different time stepping ($R=5, \beta=0, \gamma=1/2$): (a) CCT: 49×99 , (b) CCT1: 24×49 .

Table 1: The critical time stepping for different densities of grid ($R=5, \beta=0, \gamma=1/2$)

	CCT: 49×99	CCT1: 24×49	CCT2: 13×24
Δt_c (μs)	4.825×10^{-2}	10.025×10^{-2}	16.568×10^{-2}
Δt_{fem}^{lump} (μs)	5.479×10^{-2}	11.012×10^{-2}	18.138×10^{-2}
$\Delta t_c / \Delta t_{fem}^{lump}$	88.064%	91.037%	91.344%

To clarify this case further, we repeated the above steps with CCT2: 13×24 elements, and the comparison results are shown in the Table 1. The critical time step is about $16.568 \times 10^{-8} \text{s}$ in the case of CCT2, which is larger than the case of CCT1. It is hence concluded that the critical time step decreases with the increase of grid density. Besides, the critical time step of the standard FEM for the lumped mass is also listed. With more elements, the critical time step Δt_{fem}^{lump} is decreased, and this is consistent with the case of Δt_c . The values of

$\Delta t_c / \Delta t_{fem}^{lump}$ are similar, which range from 88.064% to 91.344%. As Menouillard, Réthoré, Combescure et al. (2006); Elguedj, Gravouil and Maigre (2009) suggested, $\Delta t = \frac{2}{3} \Delta t_{fem}^{lump}$ for the stationary crack, the value 2/3 is within the numerical range listed in this paper. So, the numerical stability can be guaranteed.

In addition, we took into account the effect of Newmark scheme for the critical time step. Four cases are concerned. Before studying the impact of iterative format on critical time step, all the cases are listed under the same conditions: CCT1, a mesh of 24×49 elements, $R=5$, $\Delta t = 5 \times 10^{-8}$ s. We listed the first 30 microseconds with different parameter values γ in Figure 12. An approximately identical result can be obtained. The stability conditions of the Newmark scheme are also verified directly.

In Figure 11(b), we presented the test result with $\gamma = 1/2$. As a comparison, the result with $\gamma = 2/3$ is shown in Figure 13. The divergence occur at about $10.30 \mu s$, $12.748 \mu s$, $75.168 \mu s$ when Δt is 9.000×10^{-8} s, 8.800×10^{-8} s, 8.700×10^{-8} s, respectively. The critical time we obtained is about $\Delta t_c = 8.685 \times 10^{-8}$ s, which is smaller than the case of $\gamma = 1/2$. For further investigation, the cases of $\gamma = 3/4$, $\gamma = 1$ are tested. The results are listed in Table 2. The critical time step of the standard FEM for the lumped mass are also listed. In Table 2, it is seen that the critical time step decreases with the increase of γ . So, does Δt_{fem}^{lump} . Furthermore, we observed that the values of $\Delta t_c / \Delta t_{fem}^{lump}$ are nearly the same (about 91%), and the different parameter γ have nearly no influence on the values of $\Delta t_c / \Delta t_{fem}^{lump}$.

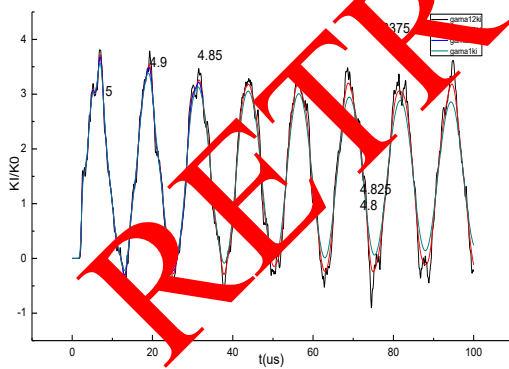


Figure: 12 Numerical results with different parameters γ (CCT1: 24×49 , $R=5$, $\beta = 0$, $\Delta t = 5 \times 10^{-8}$ s)

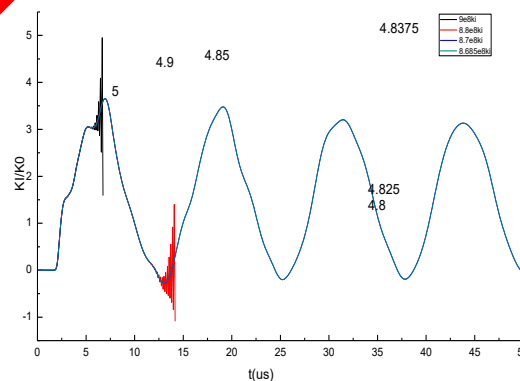


Figure: 13 Numerical stability with different time stepping (CCT1: 24×49 , $R=5$, $\beta = 0$, $\gamma = 2/3$)

Table 2: The critical time stepping for different parameters γ (CCT1: 24×49 , $R=5$, $\beta=0$)

	$\gamma=1/2$	$\gamma=2/3$	$\gamma=3/4$	$\gamma=1$
Δt_c (μs)	10.025×10^{-2}	8.685×10^{-2}	8.190×10^{-2}	7.100×10^{-2}
Δt_{fem}^{lump} (μs)	11.012×10^{-2}	9.537×10^{-2}	8.992×10^{-2}	7.787×10^{-2}
$\Delta t_c / \Delta t_{fem}^{lump}$	91.037%	91.066%	91.081%	91.178%

6 Conclusions

In the present paper, we carried out some numerical experiments of the stable explicit time stepping within the XFEM framework. A new enrichment scheme for crack tip is proposed and its applicability and availability has been sufficiently verified. The DSIF is used as an important parameter of the dynamic response and is also a parameter of judging the stability of numerical method. Objective to studying the factors that can affect the stability, different densities of grid and different parameters of Newmark scheme have been tested. The conclusions are shown as:

- The grid density and the form of iterative method have obvious effects on stability;
- The critical time stepping Δt_c decreases with the increase of grid density;
- The critical time stepping Δt_c decreases with the increase of the parameter γ between 0.5 and 1 of Newmark scheme;
- A similar conclusion can be obtained by the standard FEM with the lumped mass, and the values of $\Delta t_c / \Delta t_{fem}^{lump}$ are relatively stable.

Furthermore, the simulation results are found in good agreement with each other when they are stable. Therefore, increasing time stepping appropriately in the range of critical value can improve the computational efficiency.

Acknowledgment. The authors are grateful to the National Natural Science Foundation of China (No.11672101, No.11372099), the 12th Five-Year Supporting Plan Issue (No.2015BAB07B10), Jiangsu Province Natural Science Fund Project (No. BK20151493) and the Postgraduate Research and Innovation Projects in Jiangsu Province (No.2014B31614) for the financial support.

References

- Belytschko, T.; Black, T.** (1999): Elastic crack growth in finite elements with minimal remeshing. *International Journal for Numerical Methods in Engineering*, vol. 45, no. 5, pp. 602-620.
- Belytschko, T.; Chen, H.** (2004): Singular Enrichment Finite Element Method for

Elastodynamic Crack Propagation. *International Journal of Computational Methods*, vol. 1, no. 1, pp. 1-15.

Belytschko, T.; Chen, H.; Xu, J.; Zi, G. (2003): Dynamic crack propagation based on loss of hyperbolicity and a new discontinuous enrichment. *International Journal for Numerical Methods in Engineering*, vol. 58, no. 12, pp. 1873-1905.

Belytschko, T.; Moes, N.; Usui, S.; Parimi, C. (2001): Arbitrary discontinuities infinite elements, *International Journal for Numerical Methods in Engineering*, vol. 50, no. 4, pp. 993-1013.

Dolbow, J.; Moes, N.; Belytschko, T. (2000): Discontinuous enrichment in finite elements with a partition of unity method. *Finite Elements in Analysis and Design*, vol. 365, no. 3-4, pp. 235-260.

Duan, Q.; Song, J. H.; Menouillard, T. (2009): Belytschko. Element-local level set method for three-dimensional dynamic crack growth. *International Journal for Numerical Methods in Engineering*, vol. 80, no. 12, pp. 1520-1543.

Elguedj, T.; Gravouil, A.; Maigre, H. (2009): An explicit dynamic extended finite element method. Part 1: Mass lumping for arbitrary enrichment functions. *Computer Methods in Applied Mechanics and Engineering*, vol. 198, no. 30-32, pp. 2297-2317.

Freund, L. B. (1990): Dynamic fracture mechanics. *Cambridge Monographs on Mechanics and Applied Mathematics*.

Jim, L.; Zhang, T.; Fang, E.; Song, J. H. (2016): Explicit phantom paired shell element approach for crack branching and impact damage prediction of aluminum structures. *International Journal of Impact Engineering*, vol. 87, pp. 28-43.

Kumar, S.; Singh, I. V.; Mishra, B. K.; Singh, A. (2015): New enrichments in XFEM to model dynamic crack response of 2-D elastic solids. *International Journal of Impact Engineering*, vol. 87, pp. 193-211.

Liu, P.; Bui, T.; Zhang, C.; Yu, T. T.; Liu, G. R. et al. (2012): The singular edge-based smoothed finite element method for stationary dynamic crack problems in 2D elastic solids. *Computer Methods in Applied Mechanics & Engineering*, vol. 233-236, no. 4, pp. 68-80.

Moes, N.; Dolbow, J.; Belytschko, T. (1999): A finite element method for crack growth without remeshing. *International Journal for Numerical Methods in Engineering*, vol. 46, no. 1, pp. 431-450.

Menouillard, T.; Rethoré, J.; Combescure, A.; Bung, H. (2006): Efficient explicit time stepping for the eXtended Finite Element Method(X-FEM). *International Journal for Numerical Methods in Engineering*, vol. 68, no. 9, pp. 911-939.

Menouillard, T.; Réthoré, J.; Moës, N.; Combescure, A.; Bung, H. (2008): Mass lumping strategies for X-FEM explicit dynamics: Application to crack propagation. *International Journal for Numerical Methods in Engineering*, vol. 74, no. 3, pp. 447-474.

Menouillard, T.; Song, J. H.; Duan, Q.; Belytschko, T. (2010): Time dependent crack tip enrichment for dynamic crack propagation. *International Journal of Fracture*, vol. 62, no. 1-2, pp. 33-69.

Nagashima, T.; Omoto, Y.; Tani, S. (2003): Stress intensity factor analysis of interface cracks using X-FEM. *International Journal for Numerical Methods in Engineering*, vol.

56, no. 8, pp. 1151-1173.

Nistor, I.; Pantale, O.; Caperaa, S. (2008): Numerical implementation of the extended finite element method for dynamic crack analysis. *Advances in Engineer Software*, vol. 39, no. 7, pp. 573-587

Phan, A. V.; Gray, L. J.; Salvadori, A. (2010): Transient analysis of the dynamic stress intensity factors using SGBEM for frequency-domain elastodynamics. *Computer Methods in Applied Mechanics & Engineering*, vol. 199, no. 45-28, pp. 3039-3050.

Rabczuk, T.; Zi, G.; Gerstenberger, A.; Wall, W. A. (2008): A new crack tip element for the phantom-node method with arbitrary cohesive cracks. *International Journal for Numerical Methods in Engineering*, vol. 75, no. 5, pp. 577-599.

R  thor  , J.; Gravouil, A.; Combescure, A. (2004): A stable numerical scheme for the finite element simulation of dynamic crack propagation with re-meshing. *Computer Methods in Applied Mechanics & Engineering*, vol. 193, no. 42-44, pp. 4493-4510.

R  thor  , J.; Gravouil, A.; Combescure, A. (2005a): An energy-conserving scheme for dynamic crack growth using the eXtended finite element method. *International Journal for Numerical Methods in Engineering*, vol. 63, no. 5, pp. 651-659.

R  thor  , J.; Gravouil, A.; Combescure, A. (2005b): A combined space-time extended Finite Element Method. *International Journal for Numerical Methods in Engineering*, vol. 64, no. 2, pp. 260-284.

Song, J. H.; Belytschko, T. (2009): Dynamic fracture of shells subjected to impulsive loads. *Journal of Applied Mechanics*, vol. 76, no. 5, pp. 051301-1-9.

Song, J. H.; Belytschko, T. (2009): Cracking on node method for dynamic fracture with finite elements, *International Journal for Numerical Methods in Engineering*, vol. 77, no. 3, pp. 360-385.

Song, J. H.; Areias, P. M. A.; Belytschko, T. (2006): A method for dynamic crack and shear band propagation with phantom nodes. *International Journal for Numerical Methods in Engineering*, vol. 67, no. 6, pp. 868-893.

Tian, R.; Wen, L. (2016): Improved XFEM: An extra-dof free, well-conditioning, and interpolating XFEM. *Computer Methods in Applied Mechanics & Engineering*, vol. 285, no. 3, pp. 637-658.

Wen, L.; Tian, R. (2016): Improved XFEM: Accurate and robust dynamic crack growth simulation. *Computer Methods in Applied Mechanics & Engineering*, vol. 308, pp. 256-285.

Zi, G.; Chen, L.; Xu, J.; Belytschko, T. (2005): The extended finite element method for dynamic fractures. *Shock and Vibration*, vol. 12, no. 1, pp. 9-23.